Membrane-Mediated Peptide Conformation Change from α-Monomers to β-Aggregates

Chang-Chun Lee, Yen Sun, and Huey W. Huang*
Department of Physics and Astronomy, Rice University, Houston, Texas

ABSTRACT Jarrett and Lansbury's nucleation-dependent polymerization model describes the generic process of β-amyloid formation for a large number of diverse proteins and peptides. Here, we discuss a case of membrane-mediated nucleation that leads to β-aggregation. We studied the membrane-mediated conformation changes of the peptide penetratin, and the results of our study led us to a free-energy description for a membrane-mediated version of the Jarrett-Lansbury model. Like the prototype β-amyloid peptide Alzheimer's Aβ 1–40, penetratin is a random-coil monomer in solution but changes to α-helical or β-like conformations in the presence of anionic lipid membranes. We measured the correlations between the membrane-bound conformation of penetratin and its effect on the bilayer thickness in four different lipids with various degrees of chain unsaturation. We found a new lipid chain effect on peptide conformation. Our results showed that the interface of a lipid bilayer provided energetically favorable binding sites for penetratin in the α-helical form. However, increasing the bound molecules/lipid ratio elevated the energy level of the bound states toward a higher level that favored creation of small β-aggregates. The binding to the β-aggregate became more energetically favorable as the aggregate grew larger. The peptide aggregates were visible on the surface of giant unilamellar vesicles. Thus, membrane binding facilitates nucleation-dependent β-aggregation, which could be the prototype for the general membrane-mediated pathway to β-amyloid formation.

INTRODUCTION

The major component of Alzheimer's disease amyloid plaque, β-amyloid protein 1–40 (Aβ 1–40) (1) and the peptide penetratin (2) exhibit the same membrane-mediated conformation changes. Both peptides are random coils in solution but change to α-helical or β-like conformations in the presence of negatively charged lipid membranes. Both peptides change from α to β conformations as the lipid charge increases or as the peptide concentration increases (3–8). Since the principle behind these phenomena might clarify the molecular mechanism of β-amyloid formation, we investigated the correlation between the peptide conformation of penetratin and its effect on the membrane thickness in four different lipids with various degrees of chain unsaturation. The results revealed a new effect of membranes on penetratin, i.e., the degree of chain unsaturation influences the peptide conformation. We found that penetratin in the helical conformation was bound to the interface and thinned the membrane. In contrast, penetratin in the β-conformation had little effect on the bilayer thickness, and therefore was most likely not embedded in lipid bilayers. From the systematic results, we were able to deduce the molecular mechanism in terms of free energies, which explains the effect of membrane binding on the secondary structure of penetratin. The mechanism could be the prototype for the membrane-mediated version of nucleation-dependent amyloid formation proposed by Jarrett and Lansbury (J & L model) (1). It might explain why membrane binding has been suspected as the catalyst for polymerization leading to amyloid formation (1,9–12).

β-amyloid formation appears to be a generic process for a large number of diverse proteins and peptides (12,13). For this study, we chose the peptide penetratin, since small peptides are more likely than larger proteins to produce precise quantitative measurements. Penetratin is a 16-residue peptide corresponding to the third helix of the Antennapedia homeodomian of *Drosophila* (14). This peptide has been studied as a cell-penetrating peptide, but its purported membrane-penetrating mechanism remains controversial (15–17). We do not address the question of cell penetration here. Rather, we investigate how penetratin interacts with lipid bilayers. We believe that this is the first step toward understanding how penetratin was internalized into cells or vesicles as reported (15,16).

Penetratin is similar to antimicrobial peptides (AMPs) (18) in that both are water-soluble and spontaneously bind to membranes; however, unlike AMPs, penetratin does not form pores in the membranes (19–21). There is a long history of studying the interactions between lipid bilayers and amphipathic molecules, such as AMPs (18,22–24) and drugs (25–28). Despite the diversity of these molecules, their interactions with lipid bilayers are all characterized by strong concentration dependence. In particular, AMPs exhibit two distinct phases (24,29): at low peptide/lipid ratios, the peptides do not form pores, but at high ratios they do. We found that this concentration dependence was due to a combination of two effects, a critical micellar transition (28) from a monomeric binding phase to an oligomeric pore-forming phase, and a membrane-thinning effect that made the energy level of the monomeric phase increase

Submitted November 19, 2009, and accepted for publication February 3, 2010.

*Correspondence: hwhuang@rice.edu

Editor: Thomas J. McIntosh.

0006-3495/10/05/2236/10 $2.00

doi: 10.1016/j.bpj.2010.02.001

with the bound-molecule/lipid ratio (29). What distinguishes penetratin from the other amphipathic molecules is that it forms β-aggregates in the second phase. Nevertheless, we found important similarities between penetratin and AMPs in their interaction with lipid bilayers.

In solution, penetratin is a random coil according to its circular dichroism (CD) spectrum (5–7). In the presence of negatively charged vesicles, the CD spectra vary with the molar fraction of the charged lipids in the vesicles. At low fractions of charged lipids, the spectra are α-helical, but at high fractions they are β-like. In between, the spectra are continuous mixtures of the two (5–7). (In the literature, the β-like CD is often attributed to a β-sheet structure (3,4). Su et al. (30) called the corresponding conformation a ''turn-rich structure'' based on their NMR analysis.) The same α-to-β transition is observed if the lipid vesicles are held constant but the penetratin concentration is increased from low to high.

Beschiaschvili and Seelig (31) were the first that we know of to show that the binding of charged amphipathic peptides to oppositely charged lipid vesicles involves two kinetic equilibria. The positively charged peptides are attracted to the proximity of the negatively charged lipid headgroups according to the Poisson-Boltzmann distribution, known as the Gouy-Chapman theory (31). The peptides are subsequently bound to the lipid interface by the hydrophobic effect. If the partition coefficients (called the surface partition constant) are measured between the bound peptides and the peptide concentration in the vicinity of the charged vesicles, the values are quite independent of the lipid charge. (The apparent partition coefficients relative to the average bulk concentrations are three to five orders of magnitude larger than the surface partition constants (21,32); however, the former are not constant of concentration, whereas the latter are.) In fact, after removing the electrostatic effect, the surface partition constants for charged lipids are very close to the partition constants for neutral lipids (31,32). Very careful measurements of penetratin binding to lipid vesicles performed by Persson et al. (21) revealed the same phenomenon. Excluding the effect of electrostatic attraction, the surface partition constants of penetratin to lipid bilayers are essentially independent of the phosphocholine/phosphoglycerol ratios, indicating that the hydrophobic interactions are independent of the charged headgroups of the lipids. Thus, the effect of lipid charge is to accumulate penetratin in the vicinity of the vesicles. The apparent effect of anionic lipid charge on the conformation of penetratin (5,6,33) is essentially due to the effect of increasing peptide binding to the bilayers. The effect of increasing anionic lipid charge is the same as the effect of increasing peptide concentration. There is no independent effect of lipid charge on peptide conformation.

This leaves the main question about the peptide's β-formation to its concentration dependence. To understand how increasing the peptide concentration promotes the β-formation in the presence of lipid bilayers, we sought correlations between the peptide conformation and its effect on the membrane thickness. Previously, we found in other examples that membrane thinning played an important role in peptide-membrane interactions (24,25,27,29).

EXPERIMENT

Material and sample preparation

1,2-Dimyristoyl-*sn*-glycero-3-phosphocholine (DMPC), 1-stearoyl-2-oleoyl-*sn*-glycero-3-phosphocholine (SOPC), 1-oleoyl-2-myristoyl-*sn*-glycero-3-phosphocholine (OMPC), 1,2-dioleoyl-*sn*-glycero-3-phosphocholine (DOPC), 1,2-di-(9Z-octadecenoyl)-*sn*-glycero-3-phospho-(1′-*rac*-glycerol) (DOPG), and 1,2-dioleoyl-*sn*-glycero-3-phosphoethanolamine-N-(Lissamine Rhodamine B Sulfonyl) (Rh-DOPE) were purchased from Avanti Polar Lipids (Alabaster, AL). Penetratin (acetyl-RQIKI WFQNR RMKWK K-amide) was synthesized by GenScript (Piscataway, NJ) to >95% purity. All materials were used as delivered.

Penetratin was first dissolved in tetrafluoroethylene. Appropriate amounts of penetratin and lipid of chosen peptide/lipid molar ratio, *P*/*L*, were mixed in 1:1 (v/v) chloroform and tetrafluoroethylene, and deposited on a thoroughly cleaned flat substrate (for x-ray, 0.3 mg lipid on 1-cm^2 silicon wafers; for CD, 0.02 mg peptide on 1-cm^2 quartz plates for high *P*/*L*s, 0.2 mg of lipid on 1-cm^2 plates for low *P*/*L*s). After the solvent was removed in vacuum, the samples were hydrated by saturated water vapor at 35°C overnight (34). The results were well-aligned parallel hydrated bilayers, as proven by x-ray diffraction. The samples were kept in a temperature humidity chamber during the measurement. The DMPC experiments were performed at 33°C, and experiments on the other lipids at 25°C to ensure that all lipid-peptide bilayers were in the fluid lamellar phase (35).

X-ray lamellar diffraction

ω-2θ diffraction was collected on an Enraf Nonius Diffractus 581 and a Huber four-circle goniometer, with a line-focused Cu Kα source (λ = 1.542 Å) operating at 40 kV and 15–30 mA. The incident beam was collimated by a horizontal soller slit and two vertical slits on the front and the back sides of the soller slit. The horizontal and vertical divergence of the incident beam were 0.23° and 0.3°, respectively. The diffracted beam first passed through a vertical slit and then was discriminated by a bent graphite monochromator before entering a scintillation detector, which was biased to discriminate against higher harmonics and fluorescence. This diffractometer was designed to minimize the background signal, which in turn allowed the measurement of high diffraction orders.

An attenuator was used to prevent the first-order Bragg peak from saturating the detector. Each ω-2θ scan was performed from ω = 0.5° to ω = 6°, with a step size of $\Delta\omega$ = 0.01° (for details, see Harroun et al. (35)). The scan

was repeated three to five times for each hydration level and the results were averaged for data analysis. To use the swelling method (36) for the determination of the phases of diffraction amplitudes, each sample was scanned at several different hydration levels between 88% and 98% relative humidity (RH). Representative diffraction patterns at 98% RH are shown in Fig. 1.

The data reduction procedure has been described in many of our previous works (35,37). Briefly, the measured diffraction intensity was first corrected by the attenuator absorption and the detector's dead-time factor. After removing the background, data were corrected for absorption and diffraction volume. The integrated peak intensities were then corrected for the polarization and Lorentz factors. The relative magnitude of the diffraction amplitude was the square root of the integrated intensity. The phases were determined by the swelling method (Fig. S1 in the Supporting Material). With their phases determined, the diffraction amplitudes were Fourier transformed to obtain the bilayer electron density profile (Fig. 2). The density profile peaks at the position of the phosphate group on each side of the bilayer. Therefore, the peak-to-peak distance (PtP) corresponds to the phosphate-to-phosphate distance across the bilayer, which was used as a measure of the bilayer thickness. The errors of the PtP values (± 0.1 Å) were estimated by reproducibility using two to three independently prepared samples.

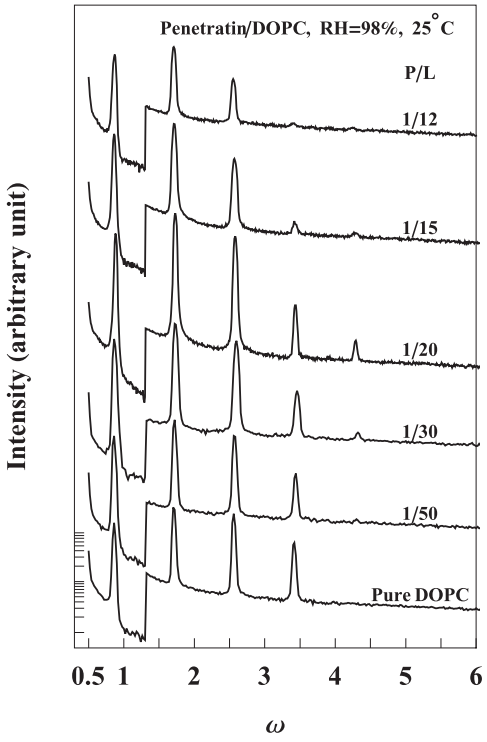

FIGURE 1 Representative diffraction patterns: series of patterns for DOPC containing penetratin at different *P*/*L* ratios, displaced vertically for clarity.

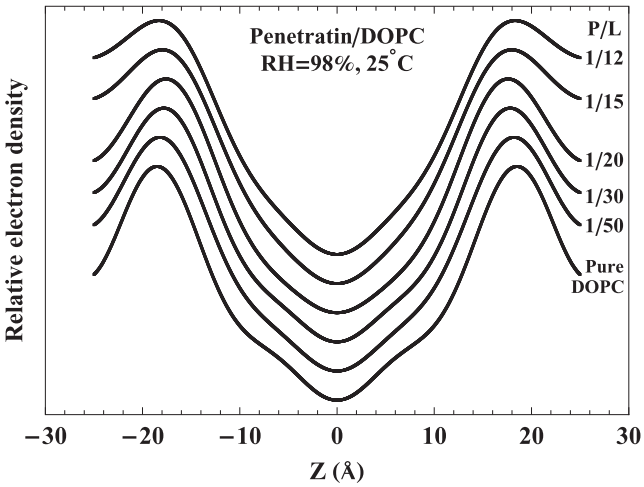

FIGURE 2 Representative electron density profiles across the bilayer in one unit cell, constructed from the data shown in Fig. 1.

CD

Spectra were measured in a Jasco (Tokyo, Japan) J-810 spectropolarimeter. The substrates were oriented normal to the incident light, as for the measurement of oriented circular dichroism (38), but no change of peptide orientation was detected during the changes of temperature or humidity. All samples were measured at the same conditions as for x-ray diffraction, i.e., 33°C for DMPC, 25°C for other lipids, and all at 98% RH. The background spectrum for each sample was the spectrum for the same amount of lipid on the same substrate. After the background correction, the spectra of different *P*/*L* for each lipid were normalized by the amount of penetratin in each sample and slightly adjusted so that all the spectra cross one isodichroic point (Fig. 3).

GUV experiment

The experiments were performed as described in Sun et al. (28). Briefly, GUVs of 7:3 DOPC/DOPG and 0.5% Rh-DOPE were produced in 210 mM sucrose solution by electroformation, and were transferred to a control chamber containing 200 mM glucose and 10 mM HEPES (pH 7.0). A GUV was aspirated by a micropipette with a small constant sucking pressure (~80 Pa, producing a membrane tension of ~0.35 mN/m) in the control chamber and then transferred to the observation chamber containing 200 mM glucose, 10 mM HEPES, and 6 M penetratin by the use of a transfer pipette. The osmolality of every solution used in the GUV experiment was measured by a Wescor Model 5520 dew-point Osmometer (Wescor, Logan, UT). Equiosmolality between the inside and outside of the GUV was maintained throughout the experiment. The video image of the process was captured by a Nikon coolSNAP HQ2 camera (Fig. 4).

A phase condenser was used to record the phase contrast between the sucrose solution inside the GUV and the glucose

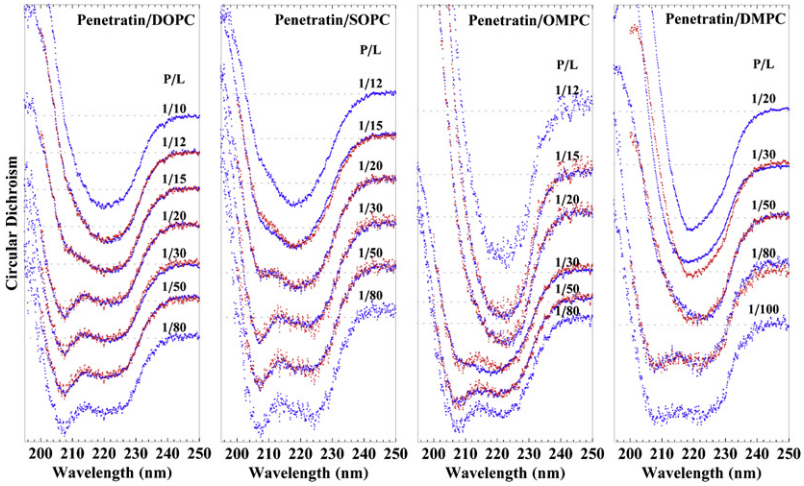

FIGURE 3 CD spectra of penetratin in four lipids as a function of *P*/*L*. The measured CD spectra are in blue; their zero lines (*dotted lines*) were displaced for clarity. For each lipid, the spectra, after the background correction, were relatively normalized to the same amount of peptide. The spectrum of the lowest *P*/*L* is defined as Spec(α) and the spectrum of the highest *P*/*L* is defined as (Spec(β)). All the spectra in between were fit by $c_1 \times$ Spec(α) + $(1 - c_1) \times$ Spec(β) (*red*). From the fit, we obtained c_1 versus *P*/*L*, as shown in Fig. 5. Reproducibility of the c_1 values from multiple samples gave $\leq$10% errors on c_1.

solution outside (not shown). We found no change in the phase contrast during the experiment, indicating that the GUV volume was constant. Under such a condition, the increase of the protrusion length inside the micropipette (Fig. 4 *b*) corresponded to an area expansion in the membrane surface; conversely, a decrease of the protrusion length (Fig. 4 *c*) corresponded to a decrease in the membrane area (28,39). Concomitant with the decrease of the protrusion length, fluorescence clumps appeared on the GUV surface (Fig. 4 *c*). This could be explained if the bound peptides formed aggregates that included lipids either by hydrophobic interaction or by electrostatic attraction between cationic peptides and lipid mixtures containing DOPG. The same experiment was repeated several times, with the same result.

RESULTS AND ANALYSIS

Four lipids were selected for this study: one of double unsaturated chains 18:1-18:1-PC (DOPC), two of single unsaturated chain 18:0-18:1-PC (SOPC) and 18:1-14:0-PC (OMPC), and one of saturated chains 14:0-14:0-PC (DMPC). Penetratin-lipid mixtures were prepared in parallel multiple bilayers on a flat substrate. We followed the principle of x-ray diffraction, which requires for correct interpretation that the samples meet appropriate conditions (40). The condition for aligned samples is called ideally imperfect, i.e., the sample should be composed of slightly misoriented, small mosaic blocks (40) (see examples in He et al.(41)). Each sample was measured by x-ray diffraction to produce the electron density profile of the bilayer at ~98% RH; above this humidity level, we found that the Bragg peaks broadened and high-order peaks diminished due to excessive layer fluctuations (37,42). In general, with samples of high *P*/*L* it was more difficult to achieve uniform alignment. All of our samples produced high-quality x-ray diffraction (Fig. 1), except for DOPC at *P*/*L* = 1:10, which, despite several attempts, diffracted poorly and was therefore not used for analysis.

Note that the electron density measured by lamellar diffraction is the density/unit length in the direction normal to the bilayer averaged over the plane of the bilayer. This density profile is overwhelmingly dominated by the lipid headgroup because of the in-plane orientation of phosphorylcholines (43) and because of the high correlation of the headgroup position from layer to layer. Interface-bound peptides do not add density to the profile, first because they take the place of headgroups and water molecules, and their normal density is not higher than that of in-plane phosphorylcholines, and second because the correlation of their positions from layer to layer is poor. As a contrast, the ions bound to the gramicidin channels produced distinct bumps in the density profile because of their layer-to-layer correlations (37), but the heavy atoms labeled to membrane-bound peptides did not (H. W. Huang, unpublished results), nor did the peptides themselves, even when they inserted into

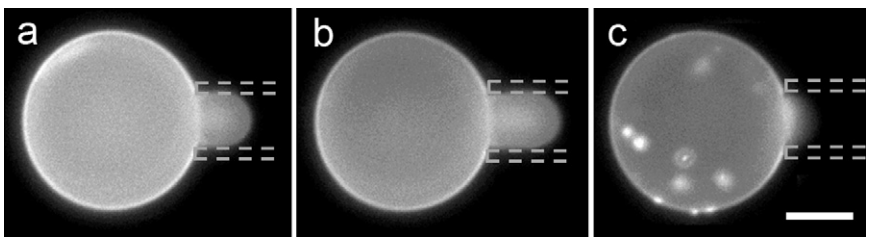

FIGURE 4 Fluorescence images of a GUV (7:3 DOPC/DOPG and 0.5% lipid dye) in a solution containing 6 μM penetratin. The dotted lines indicate the micropipette, which is not visible in the fluorescence image. (*a*) The GUV before it was exposed to penetratin. (*b*) The increasing protrusion in the micropipette indicated membrane area expansion (53). (*c*) Concomitant to the decrease in the protrusion length, bright spots appeared on the surface of the GUV, indicating the presence of peptide-lipid aggregates.

the low-density chain region (e.g., (44)). In short, peptides did not contribute to the peaks of the electron density profiles. The PtP of the profile is the average phosphate-to-phosphate distance across the bilayer (see more discussion in Huang (29)).

The multilayer alignment was not a problem for CD measurement (Fig. 3), since we were not measuring oriented CD. We note that in each lipid, the spectra were α-helix-like at low P/L, but changed to β-like as P/L increased. However, both the α-like and β-like spectra are slightly different in different lipids. Such lipid dependence has long been noted for short peptides. For example, the α-helical peptide alamethicin has slightly different CD spectra in different lipids (38,45). This is reasonable because of the end effect; the terminal regions often deviate from a continuous α-helical conformation (46) and might vary with lipid environment.

In each lipid, we assume that the spectrum of the lowest P/L is its α-helical spectrum (Spec(α)) and the spectrum of the highest P/L its β-like spectrum (Spec(β)). All the spectra in between were fit by $c_1 \times \text{Spec}(\alpha) + (1 - c_1) \times \text{Spec}(\beta)$. The fitting results were shown in Fig. 3. The fitted values of c_1 versus P/L were plotted in Fig. 5. To estimate the error for the c_1 value, we remeasured DOPC ($P/L = 1{:}20$), SOPC ($P/L = 1{:}20$), SOPC ($P/L = 1{:}15$), and DMPC ($P/L = 1{:}50$) two to three times each with independent samples. All reproduced c_1 within $\pm 10\%$. Within the errors, the CD spectra display a critical transition from α-helix-like spectra to mixtures of α- and β-spectra in each lipid (Fig. 5).

From each electron density profile (e.g., Fig. 2), the PtP was measured and plotted as a function of P/L in Fig. 6. In each lipid, the PtP initially decreased linearly with P/L until it reached a lowest PtP; it then increased approximately linearly with P/L. We designate the value of P/L corresponding to the lowest PtP by P/L^*. The values of P/L^* (Table 1) obtained from Fig. 6 are approximate, since only finite P/L points were measured. Most strikingly, the value of P/L^* is in agreement with the critical transition value of P/L at which CD spectra changed abruptly from α-helix-like to mixtures including β-spectra in each of four different lipids.

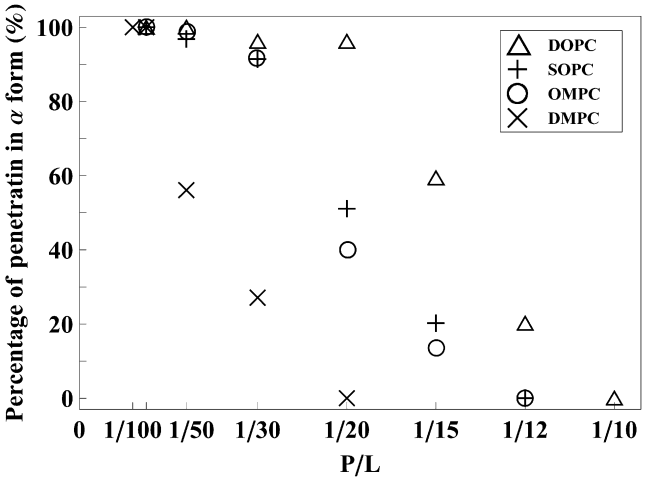

FIGURE 5 Percentage of penetratin in the α-helical form c_1 versus P/L, determined from Fig. 3.

In each panel of Fig. 6, PtP versus P/L below P/L^* was fitted with a straight line. The P/L coordinate is projected vertically upward until it intersects the fitted line and then horizontally rightward, as indicated by the dotted lines. The projected vertical coordinate of P/L was used as the coordinate of N_α/L, the number of peptides in the α-helical conformation divided by the number of lipid molecules. We then imported the data $N_\alpha/L = c_1(P/L)$ from Fig. 5. The experimental results in the $P/L < P/L^*$ region were clear: 1), the PtP values were well fitted by a straight line; and 2), the N_α/L values were close to the corresponding P/L values, indicating that all of the bound peptides were in the α-helical form and that the membrane thinning, Δ(PtP), was proportional to the amount of the α-helical bound peptides. Therefore, the N_α/L coordinate on the right-hand side of Fig. 6 can be viewed as representing the amount of α-helical bound peptides responsible for decreasing the bilayer thickness to the corresponding PtP value on the left-hand-side coordinate.

Thus, in the $P/L > P/L^*$ region, the approximate agreement between the experimental PtP on the left coordinate and N_α/L on the right coordinate of Fig. 6 indicates that even in the high P/L region, the membrane thinning was also essentially due to α-helical peptides only. Peptides in the β-conformation did not contribute to membrane thinning. Therefore, the peptides in the β-conformation were most likely not embedded in the bilayers. This is consistent with the increased density in the water region shown in the electron density profiles (Fig. 2) for $P/L = 1{:}12$ and $1{:}15$, which are above $P/L^* = 1{:}20$. Another possible reason why the β-form penetratin did not affect the membrane thickness is that it may have inserted transmembrane. However, this would require coincidental hydrophobic matching between the peptide aggregates and all four lipid bilayers (35). Considering the high charge density of penetratin (7 of 16 are positively charged), such a possibility seems unlikely.

In the third experiment, a giant unilamellar vesicle (GUV) made of 7:3 DOPC/DOPG and 0.5% lipid dye was aspirated by a micropipette and transferred to a solution containing penetratin (Fig. 4 *a*). As the peptides gradually bound to the vesicle membrane, we observed the reaction of the GUV to the increasing P/L. Initially the membrane area expanded until it reached a maximum (Fig. 4 *b*). Since membrane area expansion was equivalent to membrane thinning, this corresponded to $P/L \rightarrow P/L^*$ in Fig. 6. Then, the GUV area decreased from the maximum expanded value, corresponding to the increasing membrane thickness observed in the $P/L > P/L^*$ region in Fig. 6. Concomitant with the area decrease, aggregates began to appear on the surface of the GUV (Fig. 4 *c*). This was consistent with penetratin forming β-aggregates on the membrane surface when P/L exceeded P/L^*.

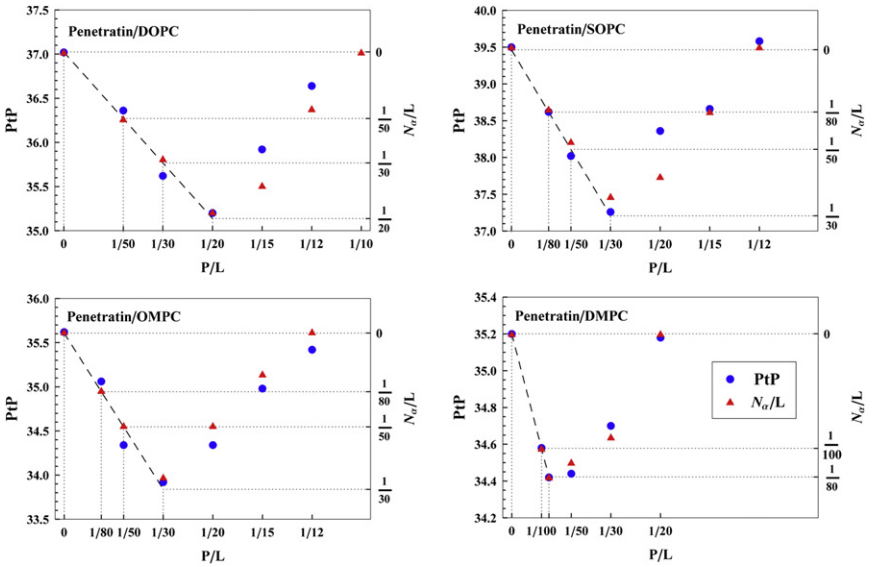

FIGURE 6 PtP versus P/L and comparison with N_α/L. The lowest PtP point defines P/L^* (Table 1). For $P/L < P/L^*$, there is a linear relation between PtP and P/L shown by the dashed line (a linear fit). The coordinate of N_α/L on the righthand ordinate was chosen to coincide with the P/L value on the dashed line so that there is a 1:1 correspondence between the PtP value and the N_α/L value on the same horizontal line. The agreement between PtP and N_α/L, for $P/L > P/L^*$, supports the assumption that membrane thinning was due to the α-helical bound peptides and that the peptides in the β-conformation did not affect the membrane thickness.

Taken together, we have high-quality data from two entirely independent experiments in striking agreement with each other in each of four arbitrarily chosen lipids. The data demonstrate that penetratin initially binds to the bilayers in the α-helical form and thins the membrane in proportion to the amount of bound peptides/lipid, P/L, until P/L reaches a critical value, P/L^*. In the region below this P/L^*, practically all of the bound peptides are in the α-helical form, i.e., $P/L \approx N_\alpha/L$. As soon as P/L exceeds P/L^*, β-form penetratin begins to appear and the percent of β-forms increases with P/L until it reaches 100%, in parallel to the membrane thinning decreasing to zero. Even in this region above P/L^*, the membrane thinning is also proportional to N_α/L, with the same proportionality as in the $P/L < P/L^*$ region.

DISCUSSION

We now try to understand the implications of the very systematic results we have obtained. What is the implication of the essentially pure α-helical region where the membrane thickness linearly decreases with P/L? What is the implication of the existence of a critical concentration, P/L^*, where the thinning is maximal and the β-form peptide begins to appear? What does it mean that in the $P/L > P/L^*$ region, where the membrane thinning decreases in proportion to the decreasing fraction of peptides in the α-form, both are in proportion to $P/L - P/L^*$, and eventually the membrane recovers to its pure bilayer thickness when all of the peptides turn into the β-form? Finally, what is the implication of the lipid chain dependence?

TABLE 1 Physical constants of penetratin bound to lipid bilayers

	A_L (Å^2)	A_s (Å^2)	P/L^*	$\epsilon^o_\alpha - \epsilon^{o*}_\beta$
DOPC (25°C)	72.7	102	1/20	$1.3k_BT$
SOPC (25°C)	67.4	155	1/30	$1.6k_BT$
OMPC (25°C)	68.8	144	1/30	$2.1k_BT$
DMPC (33°C)	61.9	155	1/65	$-0.4k_BT$

*The values of $\epsilon^o_\alpha - \epsilon^o_\beta$ are for the minimum β-aggregates.

Thermodynamics of membrane-mediated α-to-β conformation change

Amphipathic molecules typically bind to the hydrophilic-hydrophobic interface of the lipid bilayer first (29). Such bindings are characterized by a membrane thinning in proportion to the amount of bound molecules/lipid, as shown in the initial phase of penetratin binding to each lipid (Fig. 6). Previously, we called this binding phase the S phase, which has the lowest binding free energy compared with other possible binding states (29). However, since the interfacial binding stretches (increases) the membrane area (hence thinning it), it incurs an elastic energy in the lipid bilayer. As a result, the energy level of the S phase increases linearly with P/L. This has an important effect on how the peptide is distributed between the interfacial binding state and other possible binding states.

Thus, the most important characteristic of the S-phase binding is the value A_S, the monolayer area increase caused by one peptide binding. If the number of peptides bound in the S phase is N_S, the total monolayer area increase is $\Delta A = N_S A_S$. The total monolayer area of the pure lipid bilayer is $A = A_L L$, where A_L is the cross-sectional area/lipid molecule. The fractional area expansion, $\Delta A/A$, is related to the fractional thickness decrease of the hydrocarbon region, $\Delta h/h$, by the chain volume conservation (47): $\Delta A/A \approx \Delta h/h$, where the hydrocarbon thickness, h, is directly obtained from PtP by $h \approx$ PtP $-$ 10 Å (29). It follows that

$$\Delta h/h = -(A_S/A_L)(N_S/L). \quad (1)$$

Thus, the value of A_S can be measured from the initial slope of $\Delta h/h$ versus P/L. A_L can be independently measured by the chain volume (48) and h. These values are listed in Table 1.

The fractional area expansion, $\Delta A/A$, is a strain whose corresponding stress is the monolayer tension $\sigma = (K_a/2)\Delta A/A$, where $K_a/2$ is the monolayer stretch coefficient. (K_a is the bilayer stretch coefficient; its value is ~240 mN/m for most common phophatidylcholines (49)). Therefore, the energy level for the S-phase binding is given by

$$E_S = -\epsilon_S^o + \sigma A_S = -\epsilon_S^o + \left(\frac{K_a}{2}\right)\left(\frac{A_S^2}{A_L}\right)\left(\frac{N_S}{L}\right),$$

and the chemical potential by (29)

$$\mu_S = -\epsilon_S^o + \left(\frac{K_a}{2}\right)\left(\frac{A_S^2}{A_L}\right)\left(\frac{N_S}{L}\right) + k_B T \ln X_S, \quad (2)$$

where ϵ_S^o is the intrinsic binding energy of penetratin to the bilayer interface and $X_S \cong N_S/L$. The last term of Eq. 2. comes from the entropy of mixing (where k_B is the Boltzmann constant and T the temperature) following the thermodynamic theory of micellar solutions (50). This chemical potential describes the energetics of binding to the interface of a lipid bilayer by amphipathic molecules, including AMPs and amphipathic drugs (29). Since the penetratin peptides bound to the S phase are in the helical conformation, we let $\mu_S = \mu_\alpha$, $\epsilon_S^o = \epsilon_\alpha^o$, $N_S = N_\alpha$, and $E_S = E_\alpha$, for convenience in the discussion that follows.

From our CD measurements, we know that the second membrane-binding phase of penetratin is in the β-conformation. More important, our experimental data suggest that the β-states appear only at P/L concentrations above a threshold value, P/L^*, below which there are practically no peptides in the β-states. This is a strong indication that the β-states are oligomeric aggregates or, more specifically, that there are no monomeric β-states. The reason is that if there were monomeric β-states, there would have to be a significant fraction of peptides occupying such states in the $P/L < P/L^*$ region according to the Boltzmann distribution. This can be shown as follows.

Assume that the smallest β-state consists of n monomers with a chemical potential given by (50)

$$\mu_n = -n\epsilon_\beta^o + k_B T \ln X_n, \quad (3)$$

where $-\epsilon_\beta^o$ is the energy/peptide for the smallest β-state and $X_n \cong N_{\beta n}/L$; $N_{\beta n}$ is the number of n-meric β-states occupied by the peptide. As pointed out by Jarrett and Lansbury (1), the states of proteins often reflect a kinetic effect rather than that of true thermodynamic equilibrium. Before the appearance of the smallest β-states, the only bound states accessible to the peptides in solution are the interfacial binding state in the α-helical conformation and the smallest β-state. The larger β-aggregates become accessible only after the appearance of the smallest β-state. This was called the kinetic barrier of nucleation (1). Thus, in the region where $P/L < P/L^*$, the state of the peptide is determined by the quasiequilibrium condition $\mu_n = n\mu_\alpha$. This equation and the condition $N_\alpha + nN_{\beta n} = P$ determine the values of N_α and $N_{\beta n}$, and the solution can be compared with the membrane thinning data via Eq. 1, $\Delta h/h = -(A_S/A_L)(N_\alpha/L)$. The solution for N_α and $N_{\beta n}$ by curve-fitting to $\Delta h/h$ versus P/L involved three parameters: $a = (\epsilon_\alpha^o - \epsilon_\beta^o)/k_B T$, $b = K_a(A_S^2/2A_L)/k_B T$, and n. b was determined by A_S, which was in turn determined by the initial slope of $\Delta h/h$ versus P/L (K_a and A_L were already known). a and n were to be determined by solution N_α agreeing with Eq. 1 and the data. This procedure was described recently in great detail for the problem of AMPs (29).

However, there is an important difference between these two cases. For AMPs, the equilibrium condition between Eqs. 2 and 3 was assumed to be valid for the entire range of P/L, both below and above P/L^*. The curve fitting to the entire range of $\Delta h/h$ versus P/L produced a narrow range of values for parameters a and n (29). In contrast, penetratin is expected to have multiple aggregation states larger than the minimum β-state in the $P/L > P/L^*$ region, which is why the quasiequilibrium condition between Eqs. 2 and 3 is valid only for $P/L \leq P/L^*$. The data required the solution to have vanishingly small $N_{\beta n}$ (more precisely, $nN_{\beta n}/P \ll 1$) for the entire range of $P/L < P/L^*$. Although this requirement alone is insufficient to solve for the parameters a and n, it is sufficient to limit the value of n to $n \geq 4$, as demonstrated in the previous analysis (29). In other words, unless the minimum β-state is an oligomer of $n \geq 4$, it is impossible to have a finite range of P/L in which essentially no peptides are in the β-state. This is the well-known critical micellar condition (50,51). In a micellar solution, molecules remain monomers at concentrations below a threshold value called the critical micellar concentration (CMC), provided the smallest micelles consist of a sufficiently large number of monomers, $n > 15$ (29,50). In membranes, the micellar effect requires only $n \geq 4$, because the energy level of the monomeric state includes a concentration-dependent term due to membrane thinning. Thus, the important conclusion from this analysis is that membrane binding facilitates the transformation of penetratin from α-monomer to β-aggregate by elevating the energy level of the monomeric state with concentration. In Table 1, we give the values of a for the minimum aggregates $n = 4$ that produce the P/L^* for each lipid. (Note that the negative value of $\epsilon_\alpha^o - \epsilon_\beta^o$ for DMPC is not an anomaly. The antimicrobial peptide alamethicin also has a negative value of $\epsilon_\alpha^o - \epsilon_\beta^o$ (29).)

In a two-level micellar model, the monomer concentration remains constant above the CMC and all the amphiphiles in excess of CMC form monodisperse micelles (50). This is essentially the case for AMPs. Like penetratin, AMPs bound to the bilayer interface and caused membrane thinning.

When they formed pores above a critical concentration, the pores had no significant effect on the membrane thickness. As a result, the PtP versus P/L for AMPs had the characteristic of a two-level micellar model: the bilayer thickness decreased linearly with P/L up to P/L^*, and then remained practically constant above P/L^* (29), indicating that AMPs were entirely monomeric below P/L^* and that above P/L^*, the concentration of monomers remained at the critical level amid the membrane pores. The case of penetratin, as shown in Fig. 6, is very different. Below P/L^*, its behavior is identical to that of AMPs, but above P/L^*, the concentration of monomers, i.e., N_α/L, decreases more or less linearly with P/L. We believe that the reason the N_α/L decreased above P/L^* is explained by the J & L theory (1), and the reason it decreased in an approximately linear fashion is peculiar to multilayer samples.

Jarrett and Lansbury (1) proposed nucleation-dependent polymerization as the molecular mechanism for amyloid formation. In this case, the minimum size β-aggregate is the nucleus for β-aggregation. The quasiequilibrium condition used for the nucleation process in the $P/L < P/L^*$ region followed the J & L model. The subsequent binding of monomers to the aggregate is thermodynamically favorable, because monomers contact the growing aggregate at multiple sites (1). This means that the binding energy, E_β, for the monomers to the β-aggregate decreases with the growth of the aggregate, because in average the larger aggregate would present more available contact sites. According to this model, once nuclei have formed, the aggregates should grow by accumulation of monomers or by coalescence of small aggregates; until most monomers disappear (there will always be some monomers due to entropy). We suppose that this did not happen in our experiment because the mobility of peptide aggregates in lipid multilayers was increasingly limited as their size increased. Once monomers and very small aggregates had formed a sufficiently large local aggregate, the latter were more or less frozen within the matrix of lipid multilayers, preventing the formation of very large aggregates. Local aggregates grew to a size proportional to $(P/L-P/L^*)$, so that the size-dependent energy (per peptide) for the β-aggregates was on average approximately

$$E_\beta = -\epsilon_\beta^\circ - c\left(\frac{P}{L} - \frac{P*}{L}\right), \tag{4}$$

where c is a phenomenological (positive) constant. Then, the equality between the chemical potential of the aggregates and μ_α (Eq. 2) would have lowered the value of μ_α by decreasing N_α/L in proportion to $(P/L-P/L^*)$. As P/L continued to increase, eventually E_β became lower than $-\epsilon_\alpha^\circ$, and all of the bound peptides then turned into β-aggregates and the bilayer thickness recovered the value of the free lipid bilayer (Fig. 6).

Local aggregates in our samples of neutral lipids were not visible under the microscope. However, in a lipid mixture containing anionic components, the peptide aggregates were enlarged by incorporating lipids and were visible microscopically (Fig. S2). The observed uniform distribution of aggregates in the multilayer samples was consistent with the assumption of local aggregation.

Effect of unsaturated chains

How could the degree of chain unsaturation influence the β-formation of penetratin?

The formation of a nucleus is the defining characteristic of a nucleation-dependent polymerization. The J & L model (1) envisions the formation of a nucleus as the rate-determining step, because it requires a series of association steps that are thermodynamically unfavorable. What we found is that membrane binding facilitates the development of nuclei for aggregation. The interface of a lipid bilayer provides energetically favorable binding sites for penetratin in the monomeric form. However, increasing the bound molecules/lipid elevates the energy level of the bound states toward a higher level that favors creation of small β-aggregates, the nuclei for amyloid formation. This explains the observed conformation change of penetratin bound to vesicles, from α to β, as the peptide concentration increased (5–7).

If this idea is correct, qualitatively we would expect the critical concentration P/L^* to increase with the greater degree of unsaturation in the lipid chains, given the same headgroup. This is because chains with more unsaturation have larger cross-sectional areas and will provide more room in the headgroup region; therefore, a smaller strain would be created by peptide binding in the interface. This means that a larger N_α/L is required to elevate the energy level of the α bound states to the critical value, favoring the formation of small β-aggregates and hence larger P/L^*. Indeed, this was supported by the observation that $P/L^*_{\mathrm{DOPC}} > P/L^*_{\mathrm{SOPC}}$, and $P/L^*_{\mathrm{OMPC}} > P/L^*_{\mathrm{DMPC}}$ (Table 1).

The strain in the lipid bilayer was caused by the area expansion, A_S, per peptide binding. The value of A_S is roughly the cross-section of the peptide (parallel to the helical axis) minus the area vacated by the water molecules released from the lipid headgroup region during the process of peptide binding (44). The values of A_S obtained from the experimental data (Table 1) are consistent with the idea that A_S decreases as the degree of chain unsaturation increases. Thus, the lipid chain dependence discovered in this study provided supporting evidence for the membrane-mediated nucleation theory.

CONCLUDING REMARKS

As Jarrett and Lansbury (1) pointed out, it is difficult to prove a seeded polymerization model experimentally due to the near impossibility of quantifying the intermediate products during the aggregation. Although the theory is highly believable, it has so far received little direct

experimental support. Therefore, we wish to draw attention to our experimental results, which provide explicit support for the J & L model, first in demonstrating the existence of a nucleation process, and second in showing the growth of β-aggregates once the nucleus has formed. Most important, we have demonstrated the catalytic role of membrane binding in facilitating the nucleation. In contrast to amyloid formation in solution, the membrane-mediated version of the J & L model can be observed and quantified through its effect on the lipid bilayers.

Penetratin is monomeric in solution. However, even at low concentrations (e.g., 0.1 μM), it forms β-aggregates in the presence of anionic lipid vesicles. The mechanism for the formation of β-aggregates described above is not specific to penetratin. The same mechanism is likely applicable to other peptides, such as Alzheimer's Aβ 1–40, which has exhibited the same conformational changes as penetratin does with lipid charge and with peptide concentration (3,4,8). Aβ 1–40 is present extracellularly as a soluble peptide in human cerebrospinal fluid (52) at extremely low concentrations (in the nanomolar range). However, if it binds and accumulates on cell membranes, it could turn into β-amyloid through the mechanism described here.

SUPPORTING MATERIAL

Two figures are available at http://www.biophysj.org/biophysj/supplemental/S0006-3495(10)00227-4.

This work was supported by grants from the National Institutes of Health (grant No. GM55203) and the Welch Foundation (grant No.C-0991).

REFERENCES

1. Jarrett, J. T., and P. T. Lansbury, Jr. 1993. Seeding "one-dimensional crystallization" of amyloid: a pathogenic mechanism in Alzheimer's disease and scrapie? *Cell.* 73:1055–1058.
2. Derossi, D., A. H. Joliot, …, A. Prochiantz. 1994. The third helix of the Antennapedia homeodomain translocates through biological membranes. *J. Biol. Chem.* 269:10444–10450.
3. Terzi, E., G. Hölzemann, and J. Seelig. 1995. Self-association of β-amyloid peptide (1–40) in solution and binding to lipid membranes. *J. Mol. Biol.* 252:633–642.
4. Terzi, E., G. Hölzemann, and J. Seelig. 1997. Interaction of Alzheimer β-amyloid peptide(1–40) with lipid membranes. *Biochemistry.* 36:14845–14852.
5. Magzoub, M., L. E. Eriksson, and A. Gräslund. 2002. Conformational states of the cell-penetrating peptide penetratin when interacting with phospholipid vesicles: effects of surface charge and peptide concentration. *Biochim. Biophys. Acta.* 1563:53–63.
6. Magzoub, M., L. E. Eriksson, and A. Gräslund. 2003. Comparison of the interaction, positioning, structure induction and membrane perturbation of cell-penetrating peptides and non-translocating variants with phospholipid vesicles. *Biophys. Chem.* 103:271–288.
7. Lindberg, M., H. Biverståhl, …, L. Mäler. 2003. Structure and positioning comparison of two variants of penetratin in two different membrane mimicking systems by NMR. *Eur. J. Biochem.* 270:3055–3063.
8. Wong, P. T., J. A. Schauerte, …, A. Gafni. 2009. Amyloid-β membrane binding and permeabilization are distinct processes influenced separately by membrane charge and fluidity. *J. Mol. Biol.* 386:81–96.
9. Koppaka, V., C. Paul, …, P. H. Axelsen. 2003. Early synergy between Aβ42 and oxidatively damaged membranes in promoting amyloid fibril formation by Aβ40. *J. Biol. Chem.* 278:36277–36284.
10. Matsuzaki, K. 2007. Physicochemical interactions of amyloid β-peptide with lipid bilayers. *Biochim. Biophys. Acta.* 1768:1935–1942.
11. Chi, E. Y., C. Ege, …, K. Y. Lee. 2008. Lipid membrane templates the ordering and induces the fibrillogenesis of Alzheimer's disease amyloid-β peptide. *Proteins.* 72:1–24.
12. Relini, A., O. Cavalleri, …, A. Gliozzi. 2009. The two-fold aspect of the interplay of amyloidogenic proteins with lipid membranes. *Chem. Phys. Lipids.* 158:1–9.
13. Chiti, F., and C. M. Dobson. 2006. Protein misfolding, functional amyloid, and human disease. *Annu. Rev. Biochem.* 75:333–366.
14. Qian, Y. Q., M. Billeter, …, K. Wüthrich. 1989. The structure of the Antennapedia homeodomain determined by NMR spectroscopy in solution: comparison with prokaryotic repressors. *Cell.* 59:573–580.
15. Melikov, K., and L. V. Chernomordik. 2005. Arginine-rich cell penetrating peptides: from endosomal uptake to nuclear delivery. *Cell. Mol. Life Sci.* 62:2739–2749.
16. Fischer, R., M. Fotin-Mleczek, …, R. Brock. 2006. Break on through to the other side: biophyiscs and cell biology shed light on cell-penetrating peptides. *ChemBioChem.* 6:2126–2142.
17. Duchardt, F., M. Fotin-Mleczek, …, R. Brock. 2007. A comprehensive model for the cellular uptake of cationic cell-penetrating peptides. *Traffic.* 8:848–866.
18. Zasloff, M. 2002. Antimicrobial peptides of multicellular organisms. *Nature.* 415:389–395.
19. Drin, G., H. Déméné, …, R. Brasseur. 2001. Translocation of the pAntp peptide and its amphipathic analogue AP-2AL. *Biochemistry.* 40:1824–1834.
20. Thorén, P. E., D. Persson, …, B. Nordén. 2000. The antennapedia peptide penetratin translocates across lipid bilayers—the first direct observation. *FEBS Lett.* 482:265–268.
21. Persson, D., P. E. Thorén, …, B. Nordén. 2003. Application of a novel analysis to measure the binding of the membrane-translocating peptide penetratin to negatively charged liposomes. *Biochemistry.* 42: 421–429.
22. Matsuzaki, K. 1999. Why and how are peptide-lipid interactions utilized for self-defense? Magainins and tachyplesins as archetypes. *Biochim. Biophys. Acta.* 1462:1–10.
23. Shai, Y. 1999. Mechanism of the binding, insertion and destabilization of phospholipid bilayer membranes by α-helical antimicrobial and cell non-selective membrane-lytic peptides. *Biochim. Biophys. Acta.* 1462:55–70.
24. Huang, H. W. 2000. Action of antimicrobial peptides: two-state model. *Biochemistry.* 39:8347–8352.
25. Hung, W. C., F. Y. Chen, …, H. W. Huang. 2008. Membrane-thinning effect of curcumin. *Biophys. J.* 94:4331–4338.
26. Seelig, A. 2007. The role of size and charge for blood-brain barrier permeation of drugs and fatty acids. *J. Mol. Neurosci.* 33:32–41.
27. Sun, Y., W. C. Hung, …, H. W. Huang. 2009. Interaction of tea catechin (−)-epigallocatechin gallate with lipid bilayers. *Biophys. J.* 96:1026–1035.
28. Sun, Y., C. C. Lee, …, H. W. Huang. 2008. The bound states of amphipathic drugs in lipid bilayers: study of curcumin. *Biophys. J.* 95:2318–2324.
29. Huang, H. W. 2009. Free energies of molecular bound states in lipid bilayers: lethal concentrations of antimicrobial peptides. *Biophys. J.* 96:3263–3272.
30. Su, Y., R. Mani, …, M. Hong. 2008. Reversible sheet-turn conformational change of a cell-penetrating peptide in lipid bilayers studied by solid-state NMR. *J. Mol. Biol.* 381:1133–1144.
31. Beschiaschvili, G., and J. Seelig. 1990. Melittin binding to mixed phosphatidylglycerol/phosphatidylcholine membranes. *Biochemistry.* 29:52–58.

32. Wenk, M. R., and J. Seelig. 1998. Magainin 2 amide interaction with lipid membranes: calorimetric detection of peptide binding and pore formation. *Biochemistry*. 37:3909–3916.

33. Christiaens, B., S. Symoens, …, S. Vanderheyden. 2002. Tryptophan fluorescence study of the interaction of penetratin peptides with model membranes. *Eur. J. Biochem.* 269:2918–2926.

34. Ludtke, S., K. He, and H. Huang. 1995. Membrane thinning caused by magainin 2. *Biochemistry*. 34:16764–16769.

35. Harroun, T. A., W. T. Heller, …, H. W. Huang. 1999. Experimental evidence for hydrophobic matching and membrane-mediated interactions in lipid bilayers containing gramicidin. *Biophys. J.* 76: 937–945.

36. Blaurock, A. E. 1971. Structure of the nerve myelin membrane: proof of the low-resolution profile. *J. Mol. Biol.* 56:35–52.

37. Olah, G. A., H. W. Huang, …, Y. L. Wu. 1991. Location of ion-binding sites in the gramicidin channel by x-ray diffraction. *J. Mol. Biol.* 218:847–858.

38. Wu, Y., H. W. Huang, and G. A. Olah. 1990. Method of oriented circular dichroism. *Biophys. J.* 57:797–806.

39. Kwok, R., and E. Evans. 1981. Thermoelasticity of large lecithin bilayer vesicles. *Biophys. J.* 35:637–652.

40. Warren, B. E. 1969. X-ray Diffraction. Dover, Mineola, NY. 41–47, 51–54.

41. He, K., S. J. Ludtke, …, H. W. Huang. 1996. Neutron scattering in the plane of membranes: structure of alamethicin pores. *Biophys. J.* 70:2659–2666.

42. Chen, F. Y., W. C. Hung, and H. W. Huang. 1997. Critical swelling of phospholipid bilayers. *Phys. Rev. Lett.* 79:4026–4029.

43. Büldt, G., H. U. Gally, …, G. Zaccai. 1978. Neutron diffraction studies on selectively deuterated phospholipid bilayers. *Nature*. 271:182–184.

44. Lee, M. T., F. Y. Chen, and H. W. Huang. 2004. Energetics of pore formation induced by membrane active peptides. *Biochemistry*. 43:3590–3599.

45. Olah, G. A., and H. W. Huang. 1988. Circular dichroism of oriented α-helices. *J. Chem. Phys.* 89:2531–2538.

46. Fox, Jr., R. O., and F. M. Richards. 1982. A voltage-gated ion channel model inferred from the crystal structure of alamethicin at 1.5-Å resolution. *Nature*. 300:325–330.

47. Seemann, H., and R. Winter. 2003. Volumetric properties, compressibilities, and volume fluctuations in phospholipid-cholesterol bilayers. *Z. Phys. Chem.* 217:831–846.

48. Nagle, J. F., and S. Tristram-Nagle. 2000. Structure of lipid bilayers. *Biochim. Biophys. Acta*. 1469:159–195.

49. Rawicz, W., K. C. Olbrich, …, E. Evans. 2000. Effect of chain length and unsaturation on elasticity of lipid bilayers. *Biophys. J.* 79:328–339.

50. Blankschtein, D., G. M. Thurston, and G. B. Benedek. 1986. Phenomenological theory of equilibrium thermodynamic properties and phase separation of micellar solutions. *J. Chem. Phys.* 85:7268–7288.

51. Debye, P. 1949. Light scattering in soap solutions. *Ann. N. Y. Acad. Sci.* 51:575–592.

52. Seubert, P., C. Vigo-Pelfrey, …, D. Schenk. 1992. Isolation and quantification of soluble Alzheimer's β-peptide from biological fluids. *Nature*. 359:325–327.

53. Lee, M. T., W. C. Hung, …, H. W. Huang. 2008. Mechanism and kinetics of pore formation in membranes by water-soluble amphipathic peptides. *Proc. Natl. Acad. Sci. USA*. 105:5087–5092.